Beyond ray tracing for internal waves. II. Finite-amplitude effects

Geoffrey L. Brown, Andrew B. G. Bush, and Bruce R. Sutherland[a)]
Departments of Physics and of Earth and Atmospheric Sciences, University of Alberta, Edmonton, Alberta T6G 2G7, Canada

(Received 10 March 2008; accepted 4 September 2008; published online 16 October 2008)

We examine the transmission of small and moderately large internal gravity wavepackets through uniformly and nonuniformly stratified fluids using fully nonlinear numerical simulations. The simulations of finite-amplitude waves in a uniformly stratified fluid show that the weakly nonlinear theory developed for horizontally periodic wavepackets extends well to the dynamics of wavepackets with horizontal extent comparable to the horizontal wavelength. In simulations of small-amplitude wavepackets in a nonuniformly stratified fluid the transmission coefficient is found to be comparable to that computed analytically for horizontally periodic waves that radiate continuously (nontransiently) on a reflection level. Simulations of finite-amplitude waves in a nonuniformly stratified fluid show little dependence of transmission coefficient on the wavepacket extent. However, for a wide range of incident wave frequencies the simulations exhibit a monotonic increase in the transmission coefficient as a function of the incident wave amplitude. © *2008 American Institute of Physics*. [DOI: 10.1063/1.2993168]

I. INTRODUCTION

Driven by buoyancy forces, internal gravity waves propagate both vertically and horizontally through stratified fluids, transporting energy and momentum away from their source. In a dry adiabatic atmosphere, the stratification is prescribed by the rate of increase with height of the potential temperature, $\bar{\theta}(z)$. Internal waves can propagate vertically provided their intrinsic (Doppler-shifted) frequency Ω is less than the buoyancy frequency, given by $N=(g\bar{\theta}'/\theta)^{1/2}$, in which the prime denotes a z-derivative. Where $\Omega>N$ the waves are said to be evanescent. Even if generated at a small amplitude, the wave can become weakly nonlinear either as it approaches a critical level, where Ω approaches zero, or as it grows in amplitude with height due to anelastic effects. The latter results from the increase in amplitude as the wave moves upward into a less dense fluid—a consequence of momentum conservation.

At a sufficiently large amplitude the waves become unstable, thus depositing energy and momentum to the background flow. Breaking internal waves in the atmosphere are an important factor in determining the structure of the mean winds and thus atmospheric circulation patterns. Parametrizations of gravity wave drag are necessary for accurate numerical weather predictions and global climate models.[1–4] Presently, operational efficiency requires that a heuristic adaption of linear theory be employed to predict at what altitude the waves break. However, because the process of breaking is inherently nonlinear, it is important to understand how nonlinear dynamics modify the evolution of the waves so that inclusion of these effects may ultimately improve gravity wave drag parametrization schemes.

It is not the purpose of this study to examine the process of wave breaking (though see Refs. 5–7). Rather, we examine the influence of nonlinear effects on the evolution of internal waves before they reach breaking amplitudes. Ultimately the goal of this research program is to predict not how but where momentum is deposited by internal waves through consideration of nonlinear effects on wave propagation.

Although parametric subharmonic instability is one mechanism for the breakup of an internal wavepacket,[8,9] fully nonlinear numerical simulations[10] have shown that the weakly nonlinear evolution of a horizontally periodic, vertically compact internal wavepacket is dominated initially by interactions between the waves and the wave-induced mean flow (analogous to the Stokes drift for surface waves). This was confirmed by the derivation and analysis of a nonlinear Schrödinger equation governing the evolution of horizontally periodic internal wavepackets.[11,12] The equation, which filtered the wave-wave interactions associated with parametric subharmonic instability, captured well the simulated fully nonlinear evolution of the waves for over 15 buoyancy periods.[10,12]

If of sufficiently large amplitude, the wave-induced mean flow significantly Doppler shifted the waves, changing their structure and consequently changing the response of the wave-induced mean flow. Cumulatively this weakly nonlinear effect enhanced the dispersion of low-frequency waves. Conversely, the amplitude envelope of high-frequency large-amplitude waves, with $2^{-1/2}N<\Omega<N$, was found to narrow and grow in peak magnitude. These waves were also found to propagate more slowly than the vertical group velocity predicted by linear theory.

Clearly, these results put into question the reliability of linear theory in predicting where the waves grow to such large amplitude that they break. For example, as low-frequency waves grow to weakly nonlinear amplitudes, their enhanced dispersion means that the waves can propagate to

a)Author to whom correspondence should be addressed. Electronic mail: bruce.sutherland@ualberta.ca.

much larger altitudes than predicted before breaking. Likewise, high-frequency waves will break at lower altitudes than predicted by linear theory.

One purpose of the present study is to extend these results to internal wavepackets of finite horizontal extent. In this case the wave-induced mean flow acts locally only over the wavepacket extent and not over the horizontal extent of the domain. Nonetheless, as we will show, the weakly nonlinear behavior observed for horizontally periodic waves likewise occurs for horizontally localized wavepackets.

The other purpose of this study is to extend the predictions of internal wave tunneling for small-amplitude horizontally periodic waves to horizontally localized wavepackets of small and finite amplitudes. Tunneling refers to the partial transmission and partial reflection of internal waves from a vertically confined region where the waves are evanescent. Linear theory has been used[13,14] to derive analytic predictions of wave transmission across idealized piecewise-linear profiles of N and background flow $\bar{U}$. The result was generalized to predict the transmission of waves across domains with arbitrarily specified N and $\bar{U}$ profiles through integration of the Taylor–Goldstein equation. These studies were restricted to the Boussinesq approximation, in which the background density changes by a small fraction of itself over the vertical extent of the domain. A companion paper to this one[15] further extended these results to include anelastic effects but was still restricted to the study of small-amplitude waves.

As a first step toward understanding finite-amplitude effects on tunneling, we restrict ourselves here to a two-dimensional Boussinesq fluid with no background shear and we initialize the simulations with either small- or moderately large-amplitude waves. We thus form direct comparisons with the results of horizontally periodic finite-amplitude waves in a uniformly stratified fluid[12] and small-amplitude waves in a nonuniformly stratified fluid.[14] The latter study computed the transmission coefficient for upward-propagating incident waves continuously forced through the bottom of the domain. Here we must develop new diagnostic tools to account for the transient passage of the simulated wavepacket. We show that the results for small-amplitude waves are consistent with the theoretical prediction.

In Sec. II we briefly review the relevant linear theory for internal wave tunneling and the weakly nonlinear theory for horizontally periodic internal wavepackets. The numerical code used to solve the fully nonlinear equations is described in Sec. III along with the methods used to determine transmission coefficients. The results of simulations of waves in uniform and nonuniformly stratified fluids are presented in Sec. IV followed by conclusions in Sec. V.

II. THEORETICAL PRELIMINARIES

Although this work has been motivated in part by the study of waves that become weakly nonlinear as a result of anelastic growth, we restrict ourselves here to the Boussinesq approximation. Thus weakly nonlinear effects result not due to the growth of small-amplitude waves but due to the evolution of waves that are initialized to be moderately large amplitude. The study of nonlinear anelastic waves is currently under investigation and is beyond the scope of the present work.

In the Boussinesq approximation, the equations of motion for a gas and a liquid are effectively identical. For conceptual convenience we work here using density ρ rather than potential temperature θ to characterize the stratification of the fluid. In particular, the buoyancy frequency defined in terms of the background density, $\bar{\rho}(z)$, is $N=(-g\bar{\rho}'/\rho_0)^{1/2}$, in which ρ_0 is the characteristic density.

A. Small-amplitude wave transmission

The propagation of small-amplitude waves through arbitrarily specified background profiles of squared buoyancy frequency, $N^2(z)$, and horizontal flow, $\bar{U}(z)$, can be determined by ray tracing methods (e.g., see Ref. 16) where oscillatory solutions must be matched to Airy functions at reflection levels. Ray theory assumes that the waves have vertical wavelength much smaller than the scale of vertical variation of the background profiles (the WKB approximation). However, it is possible to compute the structure of the waves without this assumption through direct integration of the Taylor–Goldstein equation.[15,17]

In special circumstances, explicit analytic solutions can be determined for the structure of the waves and from these a formula for the transmission coefficient can be found. This has been done for the transmission across a hyperbolic tangent shear profile,[18] for which solutions were found in terms of hypergeometric functions. More recently, the transmission coefficient has been found for waves propagating through piecewise-linear background profiles.[13,14] The profiles were chosen so that the structure of the waves were either sinusoidal or exponential in each layer. The determination of the transmission coefficient was thus straightforward though algebraically intensive.

The results presented here in part comprise an extension to large-amplitude waves of the prediction by Sutherland and Yewchuk[13] for the transmission of small-amplitude waves in a stationary flow ($\bar{U}=0$) that propagate across an "N^2-barrier" of depth L prescribed by

$$N^2(z)=\begin{cases} N_0^2, & |z|>\dfrac{L}{2}, \\ 0, & |z|\le\dfrac{L}{2}. \end{cases} \tag{1}$$

This background state has the simplest mathematical form for the study of the partial transmission and partial reflection of the waves.

The transmission coefficient is generally defined to be the ratio of the pseudoenergy flux of the transmitted to incident waves,[14] this ratio being equivalent to the ratio of the transmitted to incident flux of wave activity. In the absence of background shear, the transmission coefficient is equivalent to the ratio of transmitted to incident wave energy.

For waves crossing the N^2-barrier defined by Eq. (1), the transmission coefficient was found to be[13]

$$T_{\text{lin}} = \left[1 + \left(\frac{\sinh(kL)}{\sin 2\Theta}\right)^2\right]^{-1}. \tag{2}$$

The corresponding reflection coefficient is $R=1-T$. Here $\Theta=\tan^{-1}(k_z/k_x)$ [so that $|\Theta|=\cos^{-1}(\Omega/N_0)$] is the angle from the vertical of lines of constant phase (equivalent to the angle from the vertical of the group velocity). Result (2) shows that for waves at a fixed relative horizontal wavenumber, kL, the maximum transmission occurs for waves with $\Theta=45°$ ($\Omega=N/\sqrt{2}$).

This result assumed that the small-amplitude waves were horizontally periodic with a fixed horizontal wavenumber k and were periodic with a fixed frequency Ω. In linear theory, a horizontal wavepacket can be Fourier decomposed in (k,Ω) space and the transmission coefficient determined for each mode. Thus the transmission of any small-amplitude wavepacket can be determined.

We will examine here the limitation of the linear theory predictions for moderately large-amplitude waves, and we extend the definition of the transmission coefficient to account for the transient interaction of a vertically compact wavepacket incident upon an N^2-barrier.

B. Weakly nonlinear effects

When waves grow to moderately large amplitudes, the superposition principle of linear theory is no longer strictly applicable. Large-amplitude effects change the manner in which internal waves evolve even in a uniformly stratified, stationary fluid. Heuristically, such effects become important if the vertical displacement amplitude of nonhydrostatic waves is greater than about 2% of the horizontal wavelength.[19]

The dominant weakly nonlinear influence that acts initially on a horizontally periodic, vertically compact wavepacket is through interactions between the waves and their wave-induced mean flow. This is the mean horizontal advection of fluid resulting from wave-wave interactions. The Stokes drift is much smaller than the horizontal group velocity of deep water waves, even for those close to breaking amplitude, and so weakly nonlinear interactions between the waves and the wave-induced mean flow can be ignored in this case. For internal waves, however, the wave-induced mean flow can be greater than the horizontal group velocity c_{gx} for waves well below overturning amplitudes. For overturning waves, the magnitude of the vertical density gradient associated with the waves exceeds the background vertical density gradient,

$$\frac{\partial}{\partial z}\rho(x,z,t) > -\frac{d}{dz}\bar{\rho}(z). \tag{3}$$

In terms of the maximum amplitude A_ξ of the vertical displacement field, the overturning condition is

$$\frac{A_\xi}{\lambda_x} > \frac{1}{2\pi}\cot\Theta, \tag{4}$$

in which λ_x is the horizontal wavelength.

Even if the initial wavepacket is statically stable, nonlinear interactions between the waves and the wave-induced mean flow can distort the wavepacket so that it evolves to become overturning.[19] Explicitly, the wave-induced mean flow associated with a horizontally periodic wavepacket is given in terms of the horizontally averaged correlation of the vertical displacement field ξ and the vorticity ζ associated with the waves,

$$\langle\mathcal{M}\rangle = -\langle\xi\zeta\rangle = -\frac{1}{\lambda_x}\int_0^{\lambda_x}\xi\zeta dx. \tag{5}$$

Using linear theory to relate the vorticity field to the vertical displacement field, the wave-induced mean flow is given by

$$U_0 = \frac{\sqrt{\pi}}{4}\frac{N_0}{k}(A_\xi k)^2\sec\Theta. \tag{6}$$

The condition for the wave-induced mean flow to drive the waves so they becoming overturning, the so-called self-acceleration condition, is $\|\mathcal{M}\| \geq c_{gx}$. Explicitly, this condition predicts that the wavepacket will evolve nonlinearly to become statically unstable if

$$\frac{A_\xi}{\lambda_x} > \frac{1}{2\pi\sqrt{2}}|\sin 2\Theta|. \tag{7}$$

Self-acceleration is the dominant mechanism for wave breaking[19] if $\Theta \lesssim 65.5°$ ($\Omega \gtrsim 0.41N$, $|m| \lesssim 2.2|k|$).

Even if condition (7) is not met, weakly nonlinear interactions between the waves and the wave-induced mean flow may nonetheless dominate the dynamics governing the evolution of a vertically compact wavepacket.[12] Subharmonic parametric instability, in which the primary waves interact nonlinearly with subharmonically excited waves, dominates the initial evolution of the waves only if they are both vertically and horizontally periodic.[20] One consequence of the weakly nonlinear dynamics is that the amplitude envelope of vertically compact wavepackets grows faster than predicted by linear theory and the vertical group velocity slows if $|\Theta| \lesssim 35.3°$ ($|m| \lesssim 0.71|k|$) provided the amplitude is sufficiently large.[12] Conversely, lower frequency large-amplitude waves disperse and the amplitude envelope decreases more rapidly than linear theory predicts.

An outstanding question is whether these results extend to wavepackets that are compact in both the horizontal and vertical directions. In this case the wave-induced mean flow acts only over the horizontal extent of the wavepacket and not over the entire horizontal domain.

Here we show that it is appropriate to define the effects of wave-wave interactions locally, producing an induced mean flow by superimposing on the initial disturbance field a perturbation horizontal velocity prescribed by

$$u(x,z,t=0) = \mathcal{M}_0 \equiv -\xi(x,z,0)\zeta(x,z,0). \tag{8}$$

The wave-induced mean flow, computed by averaging u over one wavelength, reduces to Eq. (5) if the waves are horizontally periodic.

In this study we are concerned with the propagation of waves whose amplitudes are large enough that nonlinear effects are non-negligible but are not so large that the waves eventually break during the simulation time. This restriction is particularly important regarding the computation of trans-

mission coefficients in simulations of waves incident on an N^2-barrier. If the waves break during the simulation, then the difference of the transmitted pseudoenergy flux at the top and bottom of the domain will not equal the incident pseudoenergy flux because energy will be deposited within the domain.

Thus we only perform numerical simulations where neither the overturning nor self-acceleration conditions, Eqs. (4) and (7), respectively, are satisfied. The use of these stability conditions effectively creates an upper limit on the amplitude range that will be studied.

III. NUMERICAL METHOD

A. Fully nonlinear simulation

The numerical method[21] used solves the discretized form of the following coupled, fully nonlinear equations of the total vorticity ζ_T and perturbation density ρ fields,

$$\frac{D\zeta_T}{Dt} = \frac{g}{\rho_0}\frac{\partial \rho}{\partial x} + \nu\nabla^2\zeta, \tag{9a}$$

$$\frac{D\rho}{Dt} = -w\frac{d\bar{\rho}}{dz} + \kappa\nabla^2\rho. \tag{9b}$$

Here, D/Dt is the material derivative, w is the vertical velocity, ν is the kinematic viscosity, and κ is the diffusivity.

The simulations are initialized with prescribed background fields upon which are superimposed a quasimonochromatic wavepacket and its corresponding wave-induced horizontal flow.

The background horizontal flow is constant. In practice, we set $\bar{U}=-c_{gx}$, in which c_{gx} is the horizontal group velocity. Thus small-amplitude waves stay centered horizontally in the domain. The background stratification is set to be uniform $[N(z)=N_0]$ or is prescribed with a thin unstratified layer at the center of the domain as given by Eq. (1).

Superimposed on the background is a horizontally and vertically compact Gaussian wavepacket centered a distance of $|z_0|$ below the middle of the domain. In terms of the streamfunction, this is prescribed by

$$\psi(x,z,t=0) = A_\psi e^{-(1/2)\{(x/\sigma_x)^2+[(z-z_0)/\sigma_z]^2\}}\cos(kx+mz), \tag{10}$$

where σ_x and σ_z, respectively, set the horizontal and vertical extents of the wavepacket and k and m are the horizontal and vertical wavenumbers. The waves are quasimonochromatic in the sense that we require $|\sigma_x k| \gg 1$ and $|\sigma_z m| \gg 1$. Thus we approximate the initial perturbation vorticity and density fields by $\zeta=(k^2+m^2)\psi$ and $\rho=-(\rho_0/g)N(k^2+m^2)^{1/2}\psi$, respectively. The wavenumbers and phase relationship between ζ and ρ are set so the wavepacket moves upward through the domain and rightward into the opposing wind with speed c_{gx}.

For large-amplitude waves, it is necessary to superimpose an initial horizontal velocity perturbation that is a consequence of wave-wave interactions inducing a local mean flow. This is given by Eq. (8), with ζ defined as above and $\xi=-[(k^2+m^2)^{1/2}/N]\psi$. We then superimpose on the vorticity field the vertical gradient of $\mathcal{M}_0$. (Although one could continue iteratively to use the new ζ to recompute $\mathcal{M}_0$, the correction is negligibly small for moderately large-amplitude waves.)

Although linear theory has been used to relate ζ, ρ, and ξ in terms of ψ, control simulations demonstrate that the formulas suffice even for moderately large-amplitude waves: As the waves propagate upward, the horizontally averaged flow moves upward with the waves leaving behind no residual stationary mean flow.

In practice, the length and time scales of simulations are set so that $k=1.0$ and $N_0=1.0$. However, throughout this paper we report results explicitly in terms of k and N_0 or, where convenient, the horizontal wavelength, $\lambda_x=2\pi/k$, and buoyancy period, $T_B=2\pi/N_0$.

We have run several simulations varying the vertical wavenumber, the wavepacket extent, and the amplitude. In simulations with nonuniform stratification, we additionally examine the effect of changing the depth L of the unstratified layer of fluid which is centered about $z=0$. In most simulations $\sigma_x=\sigma_z=10k^{-1}$, large enough so the waves are quasimonochromatic but still far from being horizontally periodic. In nearly all simulations the wavepacket is initially centered at $z_0=-3\sigma_z$. We examine vertical wavenumbers of $m=-0.4k$, $-0.7k$, $-1.0k$, and $-1.4k$. These span the range of modulationally stable ($|m|>2^{-1/2}k$) and unstable ($|m|<2^{-1/2}k$) wavepackets at sufficiently large amplitudes.

Control simulations were run for waves with very small initial amplitudes in order to provide a check on linear theory for waves in a uniformly stratified fluid and for waves incident on an N^2-barrier. In the latter case, the typical barrier depth was set to be $L=1.0k^{-1}$. In terms of the vertical displacement amplitude, the simulations were run by setting $A=10^{-4}\lambda_x$. In subsequent simulations the initial wavepacket amplitude was increased to values above which the wavepackets were observed to break. This limit changed depending on the value of m/k. The largest value corresponded to vertical displacement amplitude $A\simeq 0.1\lambda_x$.

In all simulations the viscosity and diffusion parameters were chosen to be so small that they negligibly influenced the wave dynamics but nonetheless ensured that the code remained numerically stable. Explicitly, we set $\nu=\kappa=10^{-4}N_0k^{-2}$, corresponding to a Reynolds number of 10 000 and a Schmidt number of 1.0.

The domain is a horizontally periodic channel with free-slip conditions on the upper and lower boundaries. The extent of the domain is set to be much larger than the extent of the wavepacket itself so that interactions with the boundaries are negligible. A domain height of $204.8k^{-1}$ was used so that the amplitude of waves at both boundaries remained small over the duration of simulations. Typically, the horizontal extent of the domain was $L_x=16\lambda_x$ ($\sim 100.5k^{-1}$) for wavepackets initialized with $\sigma_x=10k^{-1}$. The domain was proportionally larger in simulations with $\sigma_x k=20$ and 40. The basic state fields were represented at evenly spaced vertical levels of $0.05k^{-1}$ by spectral coefficients of the horizontal structure.

This vertical resolution accurately represents vertical wavenumbers of up to approximately $15.5k$. The horizontal resolution was set to resolve waves with horizontal wavenumbers up to $8k$. Simulations proceeded by advancing $0.01N_0^{-1}$ in time using a leap frog method with an Euler backstep taken at regular intervals of $0.2N_0^{-1}$. Typical simulations ran to times $t_{\max}=250N_0^{-1}$ or until the waves encountered the upper or lower boundaries. Simulations with increased resolutions and domain sizes were run and show negligible quantitative change in the resulting wavepacket evolution.

B. Wave-induced mean-flow analysis

For horizontally periodic waves, the wave-induced mean flow is given by Eq. (5). This is a function of z and t alone. The corresponding flow associated with a horizontally compact wavepacket depends on horizontal space as well as z and t. Pointwise, it is given initially by Eq. (8). The average horizontal flow induced by waves over the extent of the wavepacket as it evolves in time is estimated to be

$$\langle \mathcal{M} \rangle_\sigma(z,t) = \frac{L_x}{2\sigma_x}\left[\frac{1}{L_x}\int_0^{L_x}(-\xi\zeta)dx\right]. \tag{11}$$

The magnitude of $\langle \mathcal{M} \rangle_\sigma$ can be compared with the horizontal group velocity c_{gx} as a measure of the degree of nonlinearity of the wavepacket.

Here, we examine how the vertical structure of the wavepacket evolves over time using Eq. (11). We are primarily interested in whether the amplitude envelope is modulationally stable or unstable in the same manner as horizontally periodic waves. Some results are thus presented in terms of the relative wave-induced mean flow, $\langle \mathcal{M} \rangle_\sigma / U_0$, in which U_0, given by Eq. (6), is the maximum wave-induced mean flow at $t=0$. This normalization means that the choice of coefficient to the integral in Eq. (11) is irrelevant to the analyses of the wavepacket structure.

C. Transmission analysis

In the tunneling theory reviewed in Sec. II A, it was assumed that the incident waves were generated continuously at the lower extreme of the domain. However, in simulations of waves incident on an N^2-barrier a vertically compact wavepacket transiently reflects from and partially transmits through an unstratified layer of fluid.

To draw the connection between the theory and the simulations, we define two different measures of the transmission coefficient. The first method defines the transmission coefficient as the ratio of spatially integrated pseudoenergies:

$$T_{\mathcal{E}}(t) = \frac{\mathcal{E}_{\text{trans}}}{\mathcal{E}_{\text{total}}}, \tag{12}$$

where

$$\mathcal{E}_{\text{trans}}(t) = \int_{L/2}^{\infty}\int_{-\infty}^{\infty}\mathcal{E}(x,z,t)dxdz \tag{13a}$$

and

$$\mathcal{E}_{\text{total}}(t) = \int_{-\infty}^{\infty}\int_{-\infty}^{\infty}\mathcal{E}(x,z,t)dxdz \tag{13b}$$

are the spatially integrated pseudoenergy fields, respectively, in the transmission region (everywhere above the tunneling region) and in the entire domain.

The second method defines the transmission coefficient as the ratio of time integrated pseudoenergy fluxes,[14]

$$T_{\mathcal{F}}(t) = \frac{\mathcal{F}_{\text{trans}}}{\mathcal{F}_{\text{total}}}, \tag{14}$$

where

$$\mathcal{F}_{\text{Trans}}(t) = \int_0^{t_{\max}}\int_{-\infty}^{\infty}\mathcal{F}_z\left(x,\frac{L}{2},\tau\right)dxd\tau \tag{15}$$

is the time integrated vertical flux of pseudoenergy through the vertical level above the N^2-barrier at $z=L/2$.

The difficulty with the second method is in the determination of $\mathcal{F}_{\text{total}}$ because the entire wavepacket does not pass through a single vertical level before the leading edge has begun to reflect off the N^2-barrier and propagate in the opposite direction. To find this quantity a second control simulation is run with identical parameters to the first except that the background buoyancy frequency is constant $[N(z)=N_0]$ and $\mathcal{F}_{\text{total}}$ is defined as in Eq. (15).

Using either method the transmission varies as the wavepacket interacts with the tunneling region but eventually reaches a constant value once the bulk of the wavepacket has either reflected or transmitted. In all cases both methods give consistent results, to within 1% of each other.

IV. RESULTS

A. Propagation in a uniform stratification

Here we extend the study of weakly nonlinear horizontally periodic wavepackets[12] to the study of horizontally and vertically compact waves. We examine the evolution of the wavepacket structure by computing $\langle \mathcal{M} \rangle_\sigma(z,t)$ according to Eq. (11). The results are then transformed to a frame of reference moving at the vertical group speed predicted by linear theory. That is, the vertical coordinate is given by $Z=z-z_0-c_{gz}t$. This permits us to focus on the change in the structure of the amplitude envelope and on deviations of the vertical propagation speed from linear theory.

Figure 1 shows time-series plots of $\langle \mathcal{M} \rangle_\sigma(Z,t)/U_0$ as computed in six different simulations. These plots are presented in a way that they can be compared directly with the corresponding plots computed for horizontally periodic wavepackets[12] (i.e., in the limit $\sigma_x k \to \infty$).

Figure 1(a) shows the results of simulations in which the initial wavepacket is prescribed with vertical wavenumbers of $m=-0.4k$, $-0.7k$, and $-1.4k$ and an initial amplitude of $A_\xi=0.01\lambda_x$. In all three simulations the wave-induced mean

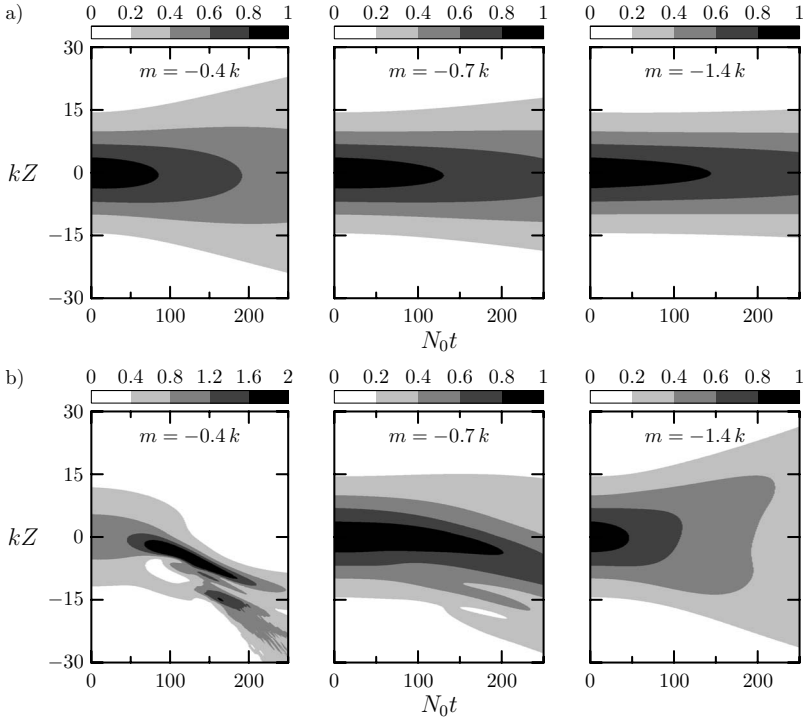

FIG. 1. The time evolution of the wave-induced mean flow, $\mathcal{M}_\sigma/U_0$ given by Eq. (8), for fully nonlinear numerical simulations of a horizontally compact wavepacket in uniform background stratification. The vertical coordinate is set to translate at the vertical group speed: $Z=z-z_0-c_{gz}t$. Wavepackets are initialized with $\sigma_x=\sigma_z=10k^{-1}$, and $m=-0.4k$, $-0.7k$, and $-1.4k$ in the left, center, and right panels, respectively. The initial amplitudes are prescribed by (a) $A_\xi=0.01\lambda_x$ and (b) $A_\xi=0.10\lambda_x$.

flow peaks along the level $Z=0$, confirming that small-amplitude wavepackets propagate upward at the vertical group speed. As the waves propagate, the vertical extent of the wavepacket broadens and the peak amplitude decreases due to linear dispersion. The dispersion is greatest in the case with $m=-0.4k$ because $|\sigma_z m|=4$ is small. In the cases with larger $|m|$, the wavepacket is closer to being monochromatic and disperses less.

Larger amplitude simulations with $A_\xi=0.08\lambda_x$ [Fig. 1(b)] show a qualitatively different behavior. In the left panel where $m=-0.4k$ the wavepacket narrows beginning at $t\approx 100N_0^{-1}$ so that the maximum value of $\mathcal{M}_\sigma$ nearly triples the initial value ($\sim 2.95U_0=2.78c_{gx}$). The vertical group speed also decreases at this time. In the right panel, for which $m=-1.4k$, the wavepacket continues to propagate at the vertical group speed. Here the wave-induced mean flow broadens more quickly and the maximum value drops by more than one-half due to nonlinear dispersive effects. The center panel shows aspects of both behaviors at the critical value of $m=-0.7k$ ($|\Theta|\sim 35°$) where the vertical group velocity is largest.

These results are consistent with simulations of horizontally periodic wavepackets[12] that demonstrated that the observed weakly nonlinear dynamics occurred due to interactions between waves and the wave-induced mean flow and not due to parametric subharmonic instability. The difference between the nonlinear evolution of horizontally compact and horizontally periodic waves is that the latter depart from linear behavior at earlier times, $t\approx 50N_0^{-1}$. This delay of the onset of weakly nonlinear dynamics for horizontally compact waves occurs because the peak wave-induced mean flow occurs only at the center of the wavepacket and decreases both horizontally and vertically away from the center.

B. Tunnelling: Wavepacket evolution

We now turn to the examination of wavepackets in nonuniform stratification for which N^2 is given by Eq. (1). First we study how weakly nonlinear effects change the wavepacket structure and in Sec. IV C we show how this changes the transmission characteristics.

The partial transmission and reflection of a wavepacket from an unstratified layer of finite depth significantly alter the evolution of a moderately large-amplitude wavepacket. The superposition of the incident and reflected wavepackets causes the maximum amplitude to increase by $1+\sqrt{R}$, where R is the reflection coefficient. Consequently the wave-induced mean flow $\mathcal{M}_\sigma$ increases by $(1+\sqrt{R})^2$. In particular, for a perfectly reflected wavepacket, the wave amplitude doubles and so the amplitude of the wave-induced mean flow quadruples.

Figure 2 shows the evolution of a small- and large-amplitude wavepackets with $m=-1.0k$ as they interact with an N^2-barrier. Snapshots of the vertical displacement field are shown at times $t=0$, $85N_0^{-1}$, and $170N_0^{-1}$ ($t\approx 0$, $13.5T_B$, and $27T_B$) for wavepackets initialized with $A_\xi=0.01\lambda_x$ [Fig. 2(a)] and $A_\xi=0.08\lambda_x$ [Fig. 2(b)].

The two leftmost panels show the initial vertical displacement field for both simulations. These appear identical because the grayscale contours span a range that is eight times larger for the large-amplitude case. The wavepacket remains approximately centered in the domain during its evolution because the background wind moves at the speed of the negative horizontal group speed, $-c_{gx}$.

At the end of both simulations the wavepacket has split into two parts: an upward-propagating transmitted portion

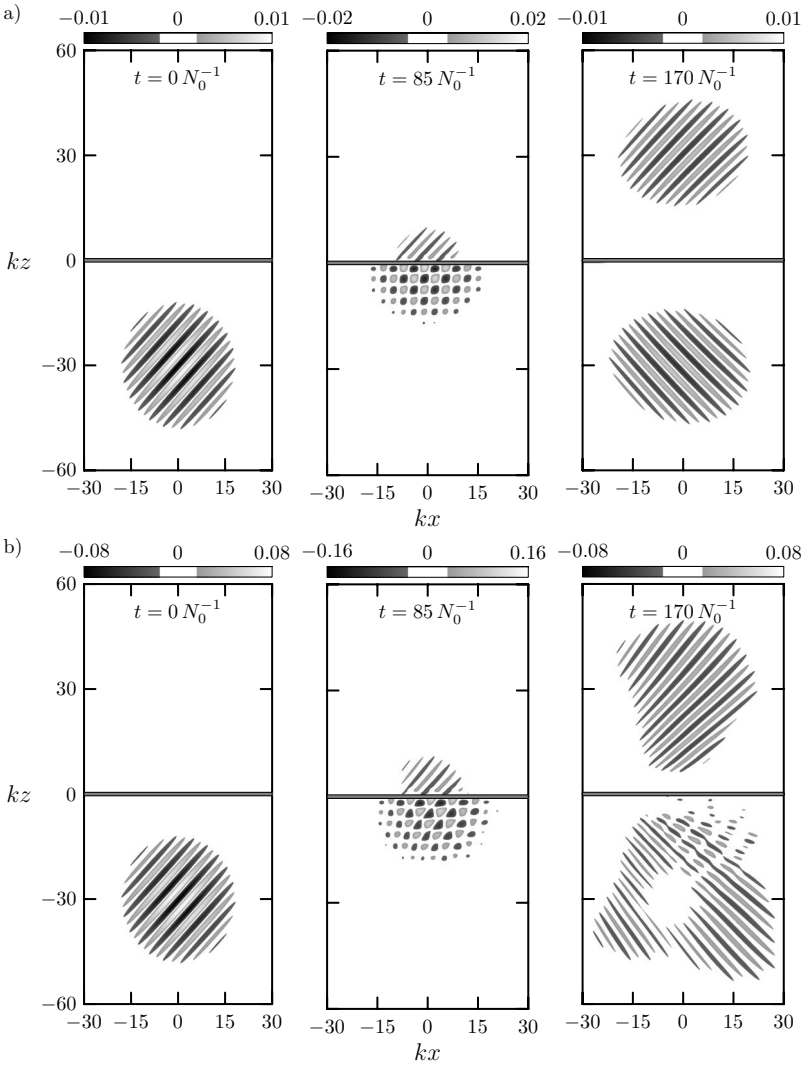

FIG. 2. Results of fully nonlinear numerical simulations of a wavepacket given initially by Eq. (10) impinging on an N^2-barrier of width $L=1.0k^{-1}$, as depicted by the gray center at $z=0$. Wavepackets are initialized with $m=-1.0k$, $\sigma_x=\sigma_z=10k^{-1}$, and (a) $A_\xi=0.01\lambda_x$ and (b) $A_\xi=0.08\lambda_x$. Grayscale contours are of the normalized vertical displacement field, ξ/λ_x, at $t=0$, $85N_0^{-1}$, and $170N_0^{-1}$ in the left, center, and right panels, respectively. The background wind moves with speed $-c_{gx}$ so that small-amplitude wavepackets should remain approximately centered in the horizontal.

and a downward-propagating reflected portion. The direction of propagation is made apparent by the tilt of the phase lines.

Focusing on the small-amplitude simulation, the center panel shows the wavepacket midway through reflecting off and tunneling through the N^2-barrier. The superposition of the incident and reflected wavepackets results in a crosshatch pattern with the maximum amplitude of vertical displacements nearly doubled. The superposition is such that heights with no vertical displacement occur at intervals of $\frac{1}{2}\lambda_z$ and columns with no vertical displacement are separated by $\frac{1}{2}\lambda_x$. The right panel shows the wavepacket after separating into the two portions. Both portions have propagated vertically at a speed nearly equal to the vertical group speed, which in this case is $|c_{gz}|\approx 0.35N_0k^{-1}$, so that the transmitted portion is centered at $z\approx 30k^{-1}$ and the reflected portion returns approximately to its initial height after $t=170N_0^{-1}$.

As well as the decrease in amplitude of the transmitted and reflected waves, the most obvious change from the initial state is the increased horizontal spread of the wavepackets. This increase is caused by the linear dispersion of the internal waves as they propagate. Unlike their horizontal extent, the vertical extent of the wavepacket is relatively unchanged, indicating that linear dispersion has a greater effect in the horizontal direction than in the vertical direction for waves with $|\Theta|=45°$. This effect is opposite for wavepackets with propagation angles smaller than $|\Theta|\sim 35°$ (not shown).

The finite-amplitude simulation in Fig. 2(b) shows several differences from the small-amplitude simulations. The partially reflected wavepacket in the center panel has a slightly different structure. The pattern remains crosshatch-like, although the shapes that make up the pattern appear more triangular than square. There are still heights with no vertical displacement at intervals of $\frac{1}{2}\lambda_z$. However, there are no longer horizontal columns with no vertical displacement. This is caused by horizontal phase shifting of the incident and reflected wavepackets due to the presence of a larger wave-induced mean flow.

Horizontal slices of the normalized vertical displacement field are shown in Fig. 3. The horizontal cross sections are taken from simulations at time $t=85N_0^{-1}$ ($t\approx 13.5T_B$) when the center of the initial wavepacket reaches the N^2-barrier. In Fig. 3(a) the initial amplitude is $A_\xi\approx 4.5\times 10^{-4}\lambda_x$ whereas in Figs. 3(b) and 3(c) the initial amplitude is $A_\xi\approx 0.081\lambda_x$. The upper panel of each figure shows grayscale contours of vertical displacement near the reflection level and the height at which the horizontal slice is taken is indicated by a dashed line.

The profiles in both Figs. 3(a) and 3(b) are for simula-

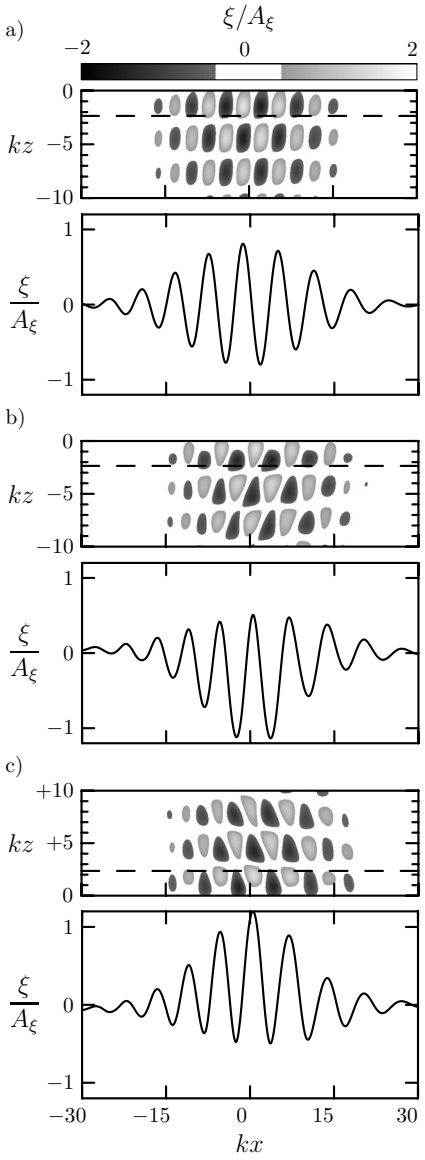

FIG. 3. Horizontal slices of the normalized vertical displacement field, ξ/A_ξ, at $t=85N_0^{-1}$, for several simulations of a wavepacket impinging on an N^2-barrier of width $L=1.0k^{-1}$. Wavepackets are prescribed by Eq. (10) with $\sigma_x=\sigma_z=10k^{-1}$. Profile (a) is taken at height $z=-\frac{3}{8}\lambda_z$ for a wavepacket initialized with $A_\xi\approx 4.5\times 10^{-4}\lambda_x$, $m=-1.0k$, and $z_0=-3\sigma_z$. Profile (b) is the same as (a) except $A_\xi\approx 0.081\lambda_x$. Profile (c) is from a downward-propagating wavepacket at height $z=\frac{3}{8}\lambda_z$ with $A_\xi\approx 0.081\lambda_x$, $m=1.0k$, and $z_0=3\sigma_z$.

tions with $m=-1.0k^{-1}$ and are taken at a height of $z=-\frac{3}{8}\lambda_z$ which is below the N^2-barrier in the reflection region. This value is chosen to lie between the heights with the maximum and minimum vertical displacement values. The small-amplitude profile shows that the horizontal wavepacket envelope maintains an approximately Gaussian envelope. The envelope remains symmetric and has a relative maximum vertical displacement of $\xi_{\max}/A_\xi=0.81$ and a relative minimum vertical displacement of $\xi_{\min}/A_\xi=-0.80$.

The large-amplitude profile in Fig. 3(b) shows a different wavepacket structure. The envelope is no longer symmetric although both the upper and lower halves retain a Gaussian shape. At the level where $z=-\frac{3}{8}\lambda_z$ the troughs of the waves are deeper and the crests less tall. Specifically, the maximum relative vertical displacement is $\xi_{\max}/A_\xi=0.51$, only 63% of the maximum measured in the small-amplitude simulation. The minimum relative vertical displacement is $\xi_{\min}/A_\xi=-1.14$, 43% lower that of the small-amplitude simulation.

The symmetry breaking was examined further by performing a simulation of a downward-propagating large-amplitude wavepacket initially centered $3\sigma_z$ above the N^2-barrier. The structure of this wavepacket above the reflection level is shown in Fig. 3(c). The structure at $z=\frac{3}{8}\lambda_z$ is a reflection of the corresponding upward-propagating wavepacket structure shown in Fig. 3(b): The crests are taller and the troughs are shallower.

In both large-amplitude simulations, the crest at the middle of the wavepacket is situated near $x=0$, a rightward phase shift from the corresponding crest in the small-amplitude simulation. This is a consequence of the wave-induced mean flow advecting the center of the large-amplitude wavepackets in the direction of the horizontal phase speed.

Finally we examine the structure of the initially upward-propagating large-amplitude wavepacket after it has reflected from the N^2-barrier as shown in the right panel of Fig. 2(b). The vertical extent of the transmitted wavepacket has spread, its trailing edge propagating at a slower vertical group speed. The reflected portion has separated into distinct wavepackets. The finite-amplitude wavepacket has undergone significant vertical and horizontal dispersions due to nonlinear effects.

The differences in wavepacket structure at large amplitudes are partially explained by examining profiles of the wave-induced mean flow given by Eq. (8) at various times. Figures 4(a) and 4(b) show the normalized wave-induced mean flow for the small- and finite-amplitude simulations examined in Fig. 2. The left panels are of the initial wave-induced mean flow given explicitly by Eq. (6). The middle panels display the largest values of the wave-induced mean flow during the simulations. This occurs just as the center of the wavepacket reaches the N^2-barrier so that the superposition of the incident and reflected wavepackets generates the largest wave amplitudes. In the small-amplitude case the maximum value is $\|\langle \mathcal{M}_\sigma \rangle\|=0.02c_{gx}$ so the effect of self-acceleration is negligible. The maximum value of the finite-amplitude flow is $\|\langle \mathcal{M}_\sigma \rangle\|=0.81c_{gx}$, which is large enough that self-acceleration effects cause the horizontal dispersion of the reflected wavepacket at later times.

One might expect the maximum amplitude of the wave-induced mean flow in the finite-amplitude case to have increased by a factor equal to the square of the wavepacket amplitude increase, in this case a factor of 64. The maximum amplitude has increased by a smaller factor than this for two reasons. The first is that the transmission coefficient is higher and therefore the reflection coefficient is smaller. The second is that the maximum amplitude of the incident wavepacket has already decreased due to dispersion by the time the wavepacket reaches the barrier. Another important feature of these profiles is the large shear due to the crosshatch pattern of the superimposed wavepackets. This shear is even greater for waves with larger $|\Theta|$ and therefore smaller vertical wavelengths.

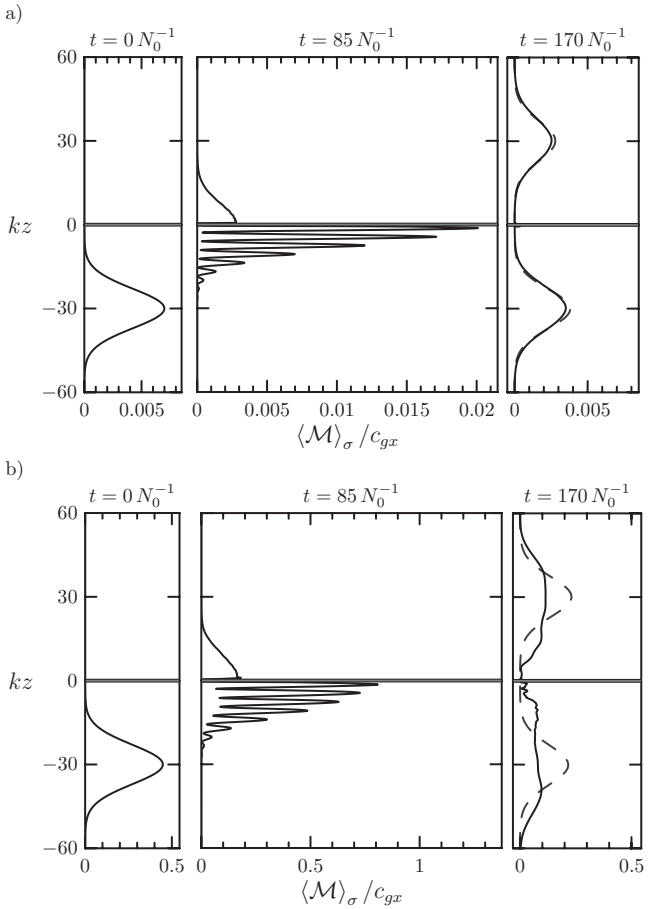

FIG. 4. The wave-induced mean flow given by Eq. (8) at various times for fully nonlinear numerical simulations. The small- and large-amplitude simulations used in (a) and (b), respectively, are the same as those used in Fig. 2. The dashed lines in the right panels represent an idealized $\mathcal{M}_\sigma$ if the transmitted and reflected wavepackets retained Gaussian shapes.

The right panels of the figure are of the wave-induced mean flow after the wavepacket has interacted with the N^2-barrier. The dashed lines represent an idealized wave-induced mean flow calculated as

$$T\langle \mathcal{M}_\sigma \rangle(z - c_{gz}t, t) + R\langle \mathcal{M}_\sigma \rangle(-z - c_{gz}t, t), \tag{16}$$

where $\mathcal{M}_\sigma(z)$ is given by Eq. (11) and T and $R = 1 - T$ are the transmission and reflection coefficients with T given by Eq. (2). Comparing this idealized flow with the calculated wave-induced mean flow in the small-amplitude case shows only a slight decrease in the maximum amplitude and a small increase in the vertical extent, confirming the lack of vertical spread due to linear dispersion. Nonlinear effects clearly enhance the dispersion, as is evident by the finite-amplitude simulation. The vertical extent of the wavepacket envelope has increased and no longer retains a Gaussian shape, although the leading edges of both the transmitted and reflected wavepackets do appear to have a Gaussian shape. This suggests that the increased vertical dispersion due to large-amplitude effects occurs beginning at the center of the wavepacket where the amplitude is largest.

The late time normalized wave-induced mean flow computed in simulations with other initial vertical wavenumbers is shown in Fig. 5. The profiles are taken at $t = 190N_0^{-1}$, $155N_0^{-1}$, and $220N_0^{-1}$ for wavepackets with $m = -0.4k$, $-0.7k$, and $-1.4k$ in the left, center, and right panels. The times are chosen so that $c_{gz}t \approx 6\sigma_z$. Again, the dashed lines show an idealized wave-induced mean-flow given by Eq. (16). Simulations for wavepackets with $m = -0.4$ and $-0.7k$ have transmitted and reflected amplitude envelopes with nearly Gaussian shape centered at heights predicted by linear theory. The peaks of each envelope in these cases are slightly lower and slower moving than the idealized prediction. Each amplitude envelope has broadened due to dispersion although the left panel shows the peak of the reflected wavepacket envelope steepening even though the maximum remains less than that of the idealized flow. This is the same behavior shown for wavepackets with $m = -0.4k$ in a uniformly stratified background. The right panel, with $m = -1.4k$, shows a qualitatively different behavior than the other two. The leading portions of the transmitted and reflected amplitude envelopes retain a Gaussian shape although they are faster moving than linearly predicted. The middle and trailing portions of both amplitude envelopes have broadened considerably from the Gaussian. The second peak of the transmitted amplitude envelope directly below the N^2-barrier is likely caused by strong shear in the wave-induced mean flow during the reflection process. Because the vertical wavelength of waves in this wavepacket is smaller than for waves with $m = -1.0k$, the gradient of the flow is even steeper than seen in the center panels of Fig. 4 and therefore the shear is larger. The strong shear contributes to the breakup of the reflected wavepacket, leaving slower moving portions near the reflection level, leading to the second peak in the wave-induced mean flow.

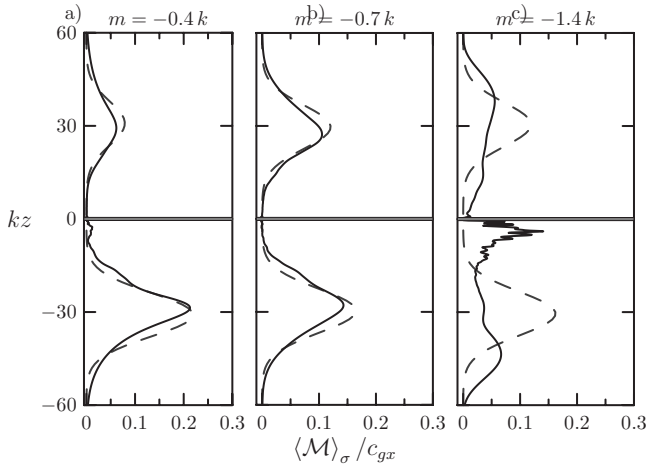

FIG. 5. The wave-induced mean flow given by Eq. (8) at late times for three simulations with varying vertical wavenumbers. Wavepackets are initialized with (a) $A_\xi = 0.045\lambda_x$ and $m = -0.4k$, (b) $A_\xi = 0.06\lambda_x$ and $m = -0.7k$, and (c) $A_\xi = 0.06\lambda_x$ and $m = -1.4k$. In all simulations $\sigma_x = \sigma_z = 10k^{-1}$ and $L = 1.0k^{-1}$. Profiles are taken at $t = 190N_0^{-1}$, $155N_0^{-1}$, and $220N_0^{-1}$ in (a), (b), and (c), respectively. The dashed lines represent an idealized $\mathcal{M}_\sigma$ where the transmitted and reflected wavepackets are Gaussian.

C. Transmission: Amplitude effects

Using Eq. (12) to calculate the fraction of the energy transmitted across the N^2-barrier for the simulation shown in Fig. 2(a), the transmission coefficient for the small-amplitude wavepacket is found to be $T = 42.3\%$, approximately 0.7%

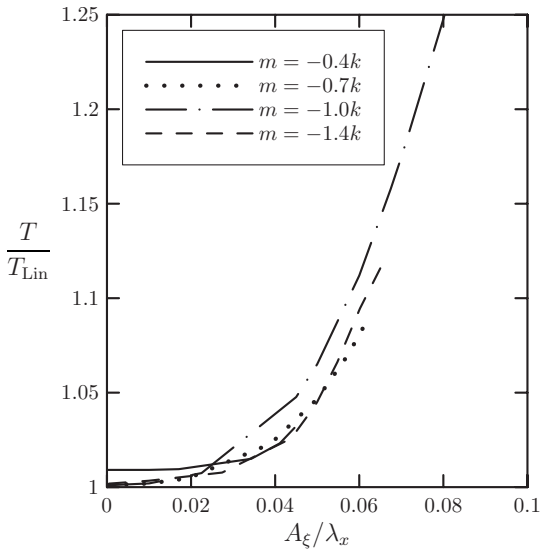

FIG. 6. Wavepacket transmission values plotted against initial amplitude for horizontally localized wavepackets prescribed initially by Eq. (10) impinging on an N^2-barrier of width $L=1.0k^{-1}$. The computed transmission values are normalized by the linearly predicted transmission values for horizontal plane waves, T_{lin}, given by Eq. (2). Wavepackets are initialized with $\sigma_x=\sigma_z=10k^{-1}$ and $m=-0.4k$ (solid line), $m=-0.7k$ (dotted line), $m=-1.0k$ (dashed-dotted line), and $m=-1.4k$ (dashed line).

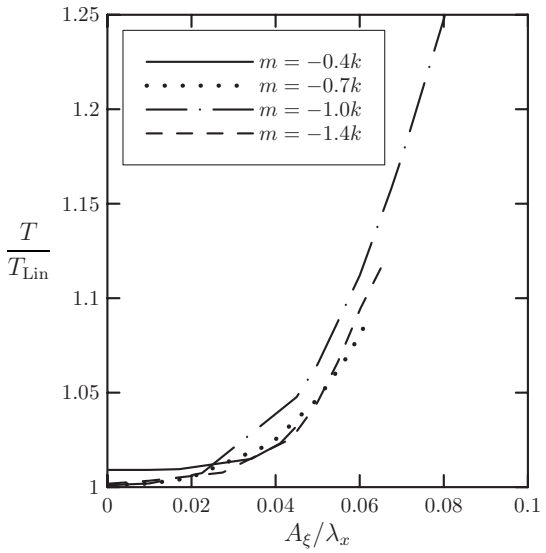

FIG. 7. As in Fig. 6 but plotting relative transmission against the relative vertical wavenumber for horizontally localized wavepackets with four different initial vertical displacement amplitudes, as indicated.

greater than the linear theory prediction for horizontal plane waves [Eq. (2)]. Thus Eq. (2) provides a good estimate of transmission even for quasimonochromatic horizontal wavepackets with σ_x as small as $10k^{-1}$.

The transmission coefficient for the corresponding finite-amplitude wavepacket simulation [Fig. 2(b)] is $T=51.6\%$, which is 22% larger than that measured for the small-amplitude wavepackets simulation and 23% larger than the linear theory prediction.

This trend, in which the transmission increases as the amplitude increases, is observed in all simulations we have performed. The transmission coefficients computed in simulations run with a range of initial amplitudes and vertical wavenumbers are plotted in Figs. 6 and 7. In all cases the barrier depth is fixed at $L=1.0k^{-1}$ and the initial wavepacket extent is given by $\sigma_x=\sigma_z=10k^{-1}$. Each line on the plot in Fig. 6 represents results computed for different initial vertical wavenumbers, as indicated on the plot. The values of m were chosen to straddle the critical value $|m|=2^{1/2}k$ below which weakly nonlinear effects can lead to growth and narrowing of the amplitude envelope and above which lead to enhanced dispersion. They also span a range about $|m|=k$, for which the transmission is predicted to be largest for a small-amplitude wavepacket. Each curve is plotted over a range of amplitudes for which the wavepacket does not break during a simulation. The self-acceleration condition, Eq. (7), dictates that waves are stable at largest amplitudes if $|m|=k$, hence why the curve corresponding to this wavenumber spans the largest range of A_ξ. This is also seen in Fig. 7 which shows the relative transmission as a function of wavenumber for wavepackets with fixed initial amplitudes.

For sufficiently small-amplitude waves, the computed transmission coefficient is close to the linear theory prediction, suggesting that even though the wavepackets are horizontally compact with $\sigma_x k=10$, the plane wave prediction is satisfactory. The discrepancies between the observed transmission and the prediction of linear theory can be attributed in part to numerical errors involved with the calculation of the transmitted wavepacket energy and due to the fact that the incident waves in the simulations are not plane waves but transient wavepackets.

The relative increase in transmission as a function of amplitude is small for $A_\xi \lesssim 0.02\lambda_x$, being within 1.5% of $T/T_{\mathrm{lin}}=1$. The relative transmission rapidly increases at larger amplitudes, the deviation being as much as 25% for wavepackets with $m=-1.0k$.

The reason for the relative increase in transmission coefficient for all wavenumbers is unclear. However, one can gain an insight as to why the peak transmission occurs for $|m|$ moderately greater than k by considering the weakly nonlinear dynamics of internal waves. For finite-amplitude waves, the wave-induced mean flow acting over the horizontal extent of the wavepacket acts to Doppler shift the waves[12] as though locally they were moving through a background with increased flow moving in the direction of k. Effectively this decreases the frequency of the incident waves. Thus waves are Doppler shifted so that $|\Theta|=\cos^{-1}(\Omega/N)$ increases. Because linear theory, given by Eq. (2), predicts that the transmission of incident plane waves is greatest if $\Theta=45°$, incident finite-amplitude waves are anticipated to have largest transmission if Θ initially is moderately smaller than 45°, that is, if $|m|$ is moderately larger than k.

Although this reasoning provides some insight into the observed behavior, a corresponding analytic prediction of the transmission is difficult to make. This is because the process of partially reflecting and transmitting from an N^2-barrier results in a complicated structure of the wave-induced mean flow as shown, for example, in Fig. 4.

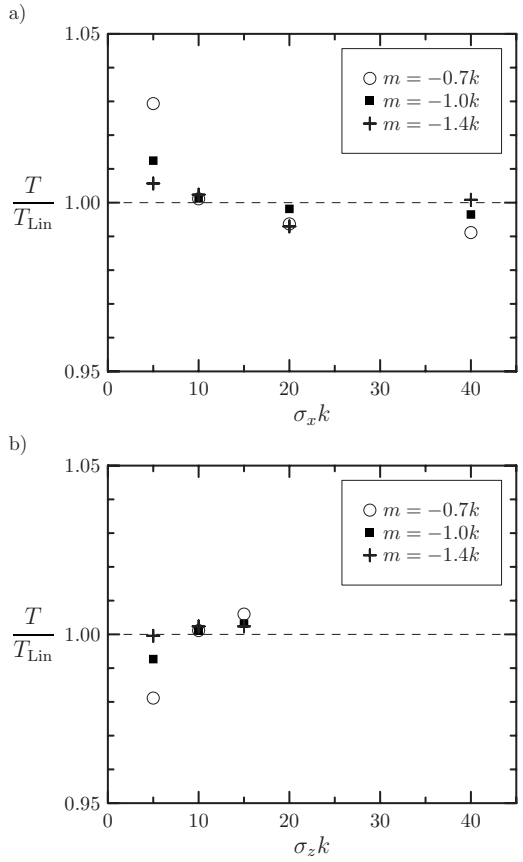

FIG. 8. Wavepacket transmission values through an N^2-barrier of width $L=1.0k^{-1}$ plotted against (a) the horizontal and (b) the vertical extent of the wavepackets for values of the vertical wavenumber as indicated. Computed transmission values are normalized by the linearly predicted transmission values for horizontal plane waves, T_{lin}, given by Eq. (2). Wavepackets are initially prescribed by Eq. (10) with $A_\psi=0.02N_0k^{-2}$ (or $A_\xi\approx 5\times 10^{-3}\lambda_x$) and in (a) $\sigma_z=10k^{-1}$ while in (b) $\sigma_x=10k^{-1}$.

D. Transmission: Wavepacket extent effects

In addition to amplitude, other initial parameters were varied to determine their impact on transmission. The effect of the extent of the wavepacket is used to determine how small a wavepacket envelope can be before results significantly deviate from the linear theory prediction for incident plane waves.

Figure 8 shows normalized transmission values calculated using Eq. (12) plotted against various wavepacket extents for several vertical wavenumbers. In all cases the initial wavepacket has a small amplitude of $A_\xi\approx 5\times 10^{-3}\lambda_x$. In Fig. 8(a) the horizontal extent is varied so that $\sigma_x=5k^{-1}$, $10k^{-1}$, $20k^{-1}$, and $40k^{-1}$ while $\sigma_z=10k^{-1}$ is kept constant. In Fig. 8(b) the vertical extent is varied so that $\sigma_z=5k^{-1}$, $10k^{-1}$, and $15k^{-1}$ while $\sigma_x=10k^{-1}$ is kept constant.

The plots show that for wavepackets with σ_x and $\sigma_z\gtrsim 10k^{-1}$ the transmission values are within 1% of the linearly predicted values for plane waves. The difference is larger for σ_x or $\sigma_z=5k^{-1}$. This result justifies the use of $\sigma_x=\sigma_z=10k^{-1}$ in other simulations because the results are consistent with plane wave solutions at small amplitudes. The first plot also shows that for $\sigma_x\lesssim 10k^{-1}$ the transmission values are greater than the plane wave predictions, whereas for $\sigma_x\gtrsim 20k^{-1}$ transmission values are less than plane wave predictions. This is reversed in the second plot where $\sigma_z\lesssim 5k^{-1}$ leads to transmission values that are less than the plane wave predictions, whereas for $\sigma_z\gtrsim 10k^{-1}$ transmission values are greater than plane wave predictions.

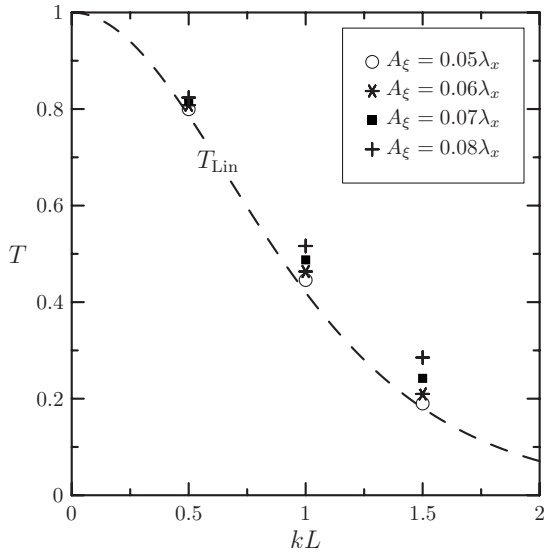

FIG. 9. Localized wavepacket transmission values plotted against N^2-barrier depths for various initial amplitudes. Wavepackets are initially prescribed by Eq. (10) with $\sigma_x=\sigma_z=10k^{-1}$ and $m=-1.0k$. The dashed line represents the linearly predicted transmission values for horizontal plane waves, T_{lin}, given by Eq. (2).

For small wavepacket extents, normalized transmission values are largest for small $|\sigma_x m|$. For all wavepacket sizes the smallest vertical wavenumber leads to the greatest deviation in transmission. For example, the wavepacket with the longest vertical wavelength ($m=-0.7k$, $\lambda_z\approx 1.4\lambda_x$) has an increase of 2.9% in transmission with $\sigma_x=5k^{-1}$.

In all cases, we expect a greater discrepancy between the analytic linear theory for plane waves and the observed transmission of small-amplitude transient wavepackets if the spatial extent of the wavepacket is comparable to the wavelength of the waves. This is because the spectral peak of the wavepacket is broader and so rigorously one would need to compute the transmission of each component of the spectrum and then form a weighted sum of the resulting transmitted energies. Research into establishing such an algorithm is currently in progress.

E. Transmission: Barrier extent effects

So far in the present work the barrier depth has been held constant at $L=1.0k^{-1}$. A range of simulations was run for other values of L that show consistent results with linear predictions. The values of L that were studied were limited by the vertical resolution. For the vertical resolution of $0.05k^{-1}$ the smallest gap examined was $L=0.5k^{-1}$ which only resolves nine vertical levels within the gap.

The transmission results for a vertical wavenumber of $m=-1.0k^{-1}$ and gap depths of $L=0.5k^{-1}$, $1.0k^{-1}$, and $1.5k^{-1}$ are shown in Fig. 9. Several amplitudes are depicted and show only a small divergence from the linear predictions. Simulations with an amplitude of $A_\xi=0.08\lambda_x$ show the larg-

est increases of 5%, 23%, and 58% in transmission values for gap widths of $0.5k^{-1}$, $1.0k^{-1}$, and $1.5k^{-1}$, respectively. In simulations with $A_\xi=0.07\lambda_x$ the transmission increases by 4%, 16%, and 34% for barrier depths of $L=0.5k^{-1}$, $1.0k^{-1}$, and $1.5k^{-1}$, respectively. These results are consistent with earlier results that show higher transmission for larger amplitude waves. The discrepancy is larger as the barrier depth increases.

V. DISCUSSION AND CONCLUSIONS

We have extended the predictions of linear theory to examine how transient and weakly nonlinear effects change the structure and transmission characteristics of horizontally and vertically compact wavepackets.

Simulations of moderately large wavepackets in a uniformly stratified fluid show that they evolve qualitatively in the same manner as horizontally periodic waves: The vertical amplitude envelope of wavepackets with small relative vertical wavenumber $|m/k|\lesssim 0.7$ narrows and grows, whereas dispersion is nonlinearly enhanced if $|m/k|\gtrsim 0.7$. This demonstrates that the dynamics are dominantly governed by weakly nonlinear interactions between the waves and the wave-induced mean flow, even though this flow acts only over the extent of the wavepacket and not over the domain as a whole. As with horizontally periodic, vertically compact internal wavepackets,[10] parametric subharmonic instability does not play an important role during the early evolution of the wavepacket.

Both the spatially integrated pseudoenergy and the time integrated pseudoenergy flux were used to quantify the transmission of transient wavepackets incident on an N^2-barrier. With length and time scales set by k and N_0, respectively, we computed the transmission as a function of the vertical wavenumber m, the wavepacket extent given by σ_x and σ_z, the vertical displacement amplitude A_ξ, and the barrier depth L.

For small-amplitude wavepackets with spatial extents as small as $\sigma_x=\sigma_z=5k^{-1}$, we found that the computed transmission agreed to within 3% of the values predicted for incident plane waves. Excellent agreement was found for $\sigma_x=\sigma_z \geq 10k^{-1}$. This provides promising evidence that theory for incident plane waves can straightforwardly be applied to transient waves.

Of primary interest was the dependence of transmission on m and A_ξ. Linear theory predicts that maximum transmission occurs for $|m/k|=1$ and weakly nonlinear theory predicts[19] that waves are stable at the largest amplitude if $|m/k|=1$. Thus we have focused on vertical wavenumbers having magnitudes close to k. A range of amplitudes was examined up to values on the cusp of wave breaking.

The structure of finite-amplitude wavepackets was found to disperse significantly after interacting with the barrier. The dispersion was greatest for wavepackets with large relative vertical wavenumbers, $|m/k|\gtrsim 1$. Nonlinear effects enhanced the dispersion of such waves as they propagated both in the uniformly stratified regions and also near the N^2 barrier where the superposition of the incident and reflected waves increased the amplitude of the disturbance and so greatly increased the magnitude of the wave-induced mean flow.

In all simulations the transmission coefficient increased as the amplitude of the incident waves increased. The discrepancy was most pronounced for waves with $|m/k|$ moderately greater than unity and for wider barrier depths.

The reason for this relative increase in transmission is not entirely clear. In part, a change is expected as a consequence of the wave-induced mean flow near the barrier acting to Doppler shift the waves initially to higher intrinsic frequencies and then lower frequencies at the packet reflects. The peak transmission of small-amplitude wavepackets occurs for waves with $|m/k|=1$ ($\Omega\sim 0.7N$). Hence, for incident large-amplitude waves with $\Omega<0.7N$, the wave-induced mean flow would Doppler shift the frequency to values closer to $0.7N$ and so enhance their transmission. But this does not explain why large-amplitude waves with low frequency, $|m/k|<1$, likewise exhibit enhanced transmission. A proper treatment of this problem requires the study of a nonlinear Schrödinger equation for internal wavepackets in nonuniform media, a study that is currently under investigation.

In brief, this study has shown that a significantly greater proportion of a finite-amplitude wavepacket is expected to penetrate through a weakly stratified region if it is nonhydrostatic with $|m/k|\simeq 1$ and if its amplitude $A_\xi\gtrsim 0.03\lambda_x$. Because enhanced transmission is not substantial for $|m/k|$ moderately larger than unity, we expect that linear theory could adequately be used in general circulation models to predict the transmission of hydrostatic waves (with $|m|\gg k$).

One should keep in mind, however, that these simulations have been restricted to waves that remain below breaking amplitudes during their evolution. Simulations of wave propagation in a uniformly stratified fluid have shown that hydrostatic internal waves disperse faster than linearly and so they are expected to break at higher altitudes than predicted by linear theory. Future work will examine the effect on transmission of a nonuniform background flow as well as nonuniform stratification. Ultimately, the intent will be to include anelastic effects so that one can examine the propagation of small-amplitude waves that become nonlinear as they move upward through a realistic atmosphere. Thus we intend to develop heuristics that can be used in general circulation models to predict more accurately where internal waves deposit their momentum.

ACKNOWLEDGMENTS

This work has been supported by the Natural Sciences and Engineering Research Council of Canada (NSERC), the Canadian Foundation for Climate and Atmospheric Science (CFCAS GR-615), and the Alberta Ingenuity Studentship program.

[1] T. N. Palmer, G. J. Shutts, and R. Swinbank, "Alleviation of a systematic westerly bias in general circulation and numerical weather prediction models through an orographic gravity drag parametrization," Q. J. R. Meteorol. Soc. **112**, 1001 (1986).
[2] N. A. McFarlane, "The effect of orographically excited gravity wave drag on the general circulation of the lower stratosphere and troposphere," J. Atmos. Sci. **44**, 1775 (1987).
[3] C. McLandress, "On the importance of gravity waves in the middle atmo-

sphere and their parameterization in general circulation models," J. Atmos. Sol.-Terr. Phys. **60**, 1357 (1998).
[4]J. F. Scinocca and N. A. McFarlane, "The parameterization of drag induced by stratified flow of anisotropic orography," Q. J. R. Meteorol. Soc. **126**, 2353 (2000).
[5]K. B. Winters and E. A. D'Asaro, "Two-dimensional instability of finite amplitude internal gravity wave packets near a critical level," J. Geophys. Res. **94**, 12709, DOI: 10.1029/JC094iC09p12709 (1989).
[6]A. S. Medvedev and G. P. Klaassen, "Vertical evolution of gravity wave spectra and the parameterization of associated wave drag," J. Geophys. Res. **100**, 25841, DOI: 10.1029/95JD02533 (1995).
[7]S. L. Vadas, M. J. Alexander, and D. C. Fritts, "Mechanism for the generation of secondary waves in wave breaking regions," J. Atmos. Sci. **60**, 194 (2003).
[8]J. Klostermeyer, "Two- and three-dimensional parametric instabilities in finite amplitude internal gravity waves," Geophys. Astrophys. Fluid Dyn. **61**, 1 (1991).
[9]P. N. Lombard and J. J. Riley, "On the breakdown into turbulence of propagating internal waves," Dyn. Atmos. Oceans **23**, 345 (1996).
[10]B. R. Sutherland, "Internal wave instability: Wave-wave vs wave-induced mean flow interactions," Phys. Fluids **18**, 074107 (2006).
[11]T. R. Akylas and A. Tabaei, "Resonant self-acceleration and instability of nonlinear internal gravity wavetrains," in *Frontiers of Nonlinear Physics*, edited by A. Litvak (Institute of Applied Physics, Nizhny Novgorod, 2005), pp. 129–135.
[12]B. R. Sutherland, "Weakly nonlinear internal wavepackets," J. Fluid Mech. **569**, 249 (2006).
[13]B. R. Sutherland and K. Yewchuk, "Internal wave tunnelling," J. Fluid Mech. **511**, 125 (2004).
[14]G. L. Brown and B. R. Sutherland, "Internal wave tunnelling through non-uniformly stratified shear flow," Atmos.-Ocean. **45**, 47 (2007).
[15]J. T. Nault and B. R. Sutherland, "Beyond ray tracing for internal waves. I. Small-amplitude anelastic waves," Phys. Fluids **20**, 106601 (2008).
[16]M. J. Lighthill, *Waves in Fluids* (Cambridge University Press, Cambridge, 1978).
[17]J. T. Nault and B. R. Sutherland, "Internal wave tunnelling across a mixed region," Phys. Fluids **19**, 016601 (2007).
[18]C. A. Van Duin and H. Kelder, "Reflection properties of internal gravity waves incident upon a hyperbolic tangent shear layer," J. Fluid Mech. **120**, 505 (1982).
[19]B. R. Sutherland, "Finite-amplitude internal wavepacket dispersion and breaking," J. Fluid Mech. **429**, 343 (2001).
[20]B. R. Sutherland, "Rayleigh wave-internal wave coupling and internal wave generation above a model jet stream," J. Atmos. Sci. **63**, 1042 (2006).
[21]B. R. Sutherland and W. R. Peltier, "Turbulence transition and internal wave generation in density stratified jets," Phys. Fluids **6**, 1267 (1994).